Geothermics 116 (2024) 102833

Contents lists available at ScienceDirect

Geothermics

journal homepage: www.elsevier.com/locate/geothermics

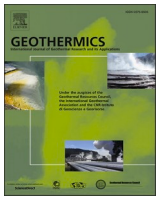

# Fracture characterisation using 3-D seismic reflection data for advanced deep geothermal exploration in the NE German Basin

Asrillah Asrillah [a,b,c,*], Agus Abdullah [d], Klaus Bauer [a], Ben Norden [a], Charlotte M. Krawczyk [a,b]

[a] German Research Centre for Geosciences (GFZ), Potsdam, Germany
[b] Institute for Applied Geosciences, Technische Universität Berlin (TUB), Germany
[c] Department of Geophysical Engineering, Universitas Syiah Kuala (USK), Banda Aceh, Indonesia
[d] Department of Geophysical Engineering, Universitas Pertamina (UP), Jakarta, Indonesia

ARTICLE INFO

*Keywords:*
3-D seismic-reflection-data
Zechstein-salt
Fracture
Anisotropy
Velocity-Variation-with-Azimuth
Northeast-German-Basin

ABSTRACT

At the geothermal research platform Gross Schönebeck (NE German Basin), we analysed 3-D seismic reflection data to determine the degree and direction of azimuthal velocity anisotropy which is interpreted as the effect of sub-vertical fracturing. Above the Zechstein salt, the observed anisotropy roughly correlates to fault structures formed by an upwelling salt pillow. Below the salt, faults are not obvious and the direction of less pronounced anisotropy and interpreted fracturing follows the trend of the regional stress field. The fracturing in an extensional setting above salt pillows may cause higher permeability and better conditions for geothermal exploitation.

## 1. Introduction

Comprehensive information about subsurface natural fractured reservoir characteristics is especially important for prospection and subsurface utilization, for instance for geothermal energy engineering (e.g., Wenke et al., 2010; Grant, 2013; Faulds and Hinz, 2015; Lepillier et al., 2019), because fractures can act as channels for fluid flow enhancing hydraulic permeability if the fractures are open and conductive for fluids (Stober and Bucher, 2014 and 2015; Bakulin et al., 2000; Shapiro and Kaselow, 2005) or need to be considered in stimulation concepts. The degree and direction of natural fracturing is related with an anisotropy signature of the rock matrix. Both parameters are relevant to develop reservoir models with preferred directions and magnitudes of hydraulic permeability.

While borehole data allows direct access to lithology and reservoir properties, such as porosity and permeability, 3-D seismic field experiments with different layouts of source and receiver setup are applied to optimize drilling strategies ahead of the operation, and to minimize the risk of unsuccessful geothermal exploitation in an area (Liu and Martinez, 2012; Aleardi et al., 2015; Lüschen et al., 2015; von Hartmann et al., 2015; Bauer et al., 2017; Krawczyk et al., 2019; Wawerzinek et al., 2021). However, fault zones and fracture networks often bear an inherent small-scale complexity close to the seismic resolution, so that it is difficult to resolve them directly from the data. For this purpose, various options for attribute analyses e.g., coherence, curvature, RMS amplitude and instantaneous frequencies, ant-tracking analysis, spectral decomposition using wavelet transform, impedance inversion and crossplots (Gazar et al., 2011; Suo et al., 2012; Pussak et al., 2014; Marfurt, 2018; Ziesch et al., 2019; Bauer et al., 2020; Wadas and von Hartmann, 2022; Wadas et al., 2023) and numerical modelling, such as 3-D palinspastic reconstruction (LaPointe et al., 2002), exist to better explore the sub-seismic scale of fracture networks (Krawczyk et al., 2015).

Approaches considering Amplitude Variation with Offset or Azimuth (AVO, AVA respectively) as well as Velocity Variation with Azimuth (VVA) have widely been implemented for hydrocarbon exploration (e.g., Lynn et al., 1999; Hall and Kendall, 2003; Al-Marzoug et al., 2006; Lüschen et al., 2014; Aleardi et al., 2015; Schmelzbach et al., 2016), especially to identify fracture-induced anisotropy (Garotta, 1989; Alkhalifah et al., 1995; Craft et al., 1997; Li et al., 1999; Bakulin et al., 2000; Jenner et al., 2001; Shen et al., 2002; Shouli et al., 2007; Wang et al., 2007; Gray, 2007; Liu et al., 2014).

In this study, we apply the VVA approach for the first time to geothermal reservoir data and show along the 3-D reflection seismic data at the geothermal research platform Groß Schönebeck (Krawczyk et al., 2019) how the fracture properties of different subsurface layers

* Corresponding author.
*E-mail address:* asrillah@gfz-potsdam.de (A. Asrillah).

https://doi.org/10.1016/j.geothermics.2023.102833
Received 23 June 2023; Received in revised form 26 August 2023; Accepted 25 September 2023
Available online 6 October 2023

relevant to potential geothermal utilization can be evaluated in terms of presence, intensity, and orientation.

## 2. Geological setting

The Geothermal Research Platform Groß Schönebeck is located in the Northeast German Basin (NEGB), ca. 50 km north of Berlin (Fig. 1). The study area underwent different geodynamic phases encompassing Caledonian and Variscan collision tectonics, Rotliegend volcanism and Mesozoic basin development (see reviews in Krawczyk et al., 2008a, b and Doornenbal and Stevenson, 2010 with references therein). In the course of this, the stress field varied and probably produced faults and fractured reservoir compartments (Marotta et al., 2001; 2002).

The geology in the study area shows the typical lithology expected in the North German Basin (Hoth et al., 1993; Norden et al., 2023 and references therein). After late Carboniferous thermal relaxation, sedimentation provided thick deposits of up to 6 km, consisting often of thick Permian (Rotliegend and Zechstein, ca. 2 km thick), Triassic (ca. 1.5 km thick), and Jurassic sediments.

The thickness of the Mesozoic sequences is quite variable within the basin and depends on the local structural setting, especially for the Cretaceous and Tertiary deposits. Fractures as indicators for present or ancient stress regimes in the North German Basin were analysed by several authors (e.g., Röckel and Lempp, 2003; Blöcher et al., 2016 and Nadoll et al., 2019) showing that the ductile Zechstein salt causes a decoupling of the stress field with a more regional component below and a more variable local stress field above the Zechstein deposits. Thus, fracture analysis of zones above the Zechstein unit is likely to show a different fracture pattern than analysis for zones below the Zechstein, like the Permian Rotliegend.

The North German Basin represents a low-enthalpy setting requiring deep boreholes to reach higher temperatures needed for electricity generation – meeting petrothermal conditions at great depths (> 4 km). A hydrothermal utilization, like applied in the other two geothermal type localities in Germany (Molasse Basin, Upper Rhine graben; Agemar et al., 2014), is therefore often restricted to shallower depths with lower temperatures (below 100 °C) in the North German Basin. At the Groß Schönebeck site, two geothermal boreholes focused on Permo-Carboniferous reservoir targets provide more details that can be traced by 3-D seismic data into the surrounding (Krawczyk et al., 2019; Fig. 1). To investigate the suitability of this deeper geothermal system for power generation, the Permo-Carboniferous targets were tested for hydraulic fracturing in wells (Holl et al., 2005; Legarth et al., 2005; Zimmermann et al., 2011; Blöcher et al., 2016), and for facies discrimination using seismic data (Bauer et al., 2020; Norden et al., 2023).

While information about the spatial distribution of natural fractured reservoir characteristics at the site were derived from 2-D seismic models and geological concepts before (Moeck et al., 2009b), we use new 3-D seismic data (Krawczyk et al., 2019) in this study to derive information on possible fractures and fracture orientations for four seismically well-traceable horizons at Groß Schönebeck.

The studied reflector horizons from top to bottom with lithological types (see in detail Fig. 1b for reference) comprise stratigraphic horizons from the Mesozoic (S1), top of Zechstein (X1), base of Zechstein (Z1) and close to the Rotliegend Elbe Reservoir Sandstone (ERS). As shown in Fig. 1b, the depth and time domain of the target horizons are as follow. The S1 reflector within the Upper Buntsandstein formation is seated at ca. 1600–2400 m depth (equivalent to 1.1–1.6 s two-way-traveltime, twt), the Zechstein salt body characterized by the horizons X1 and Z1 occurs at 2400–3800 m depth (ca. 1.6–2.1 s twt), and a horizon within the sedimentary Rotliegend is located at about 4050 m depth (2.3 s twt). For details of horizon definition, see also Reinhardt (1993), Krawczyk et al. (2019) and Norden et al. (2023). The analysed target horizons are roughly sketched in Fig. 2 and are derived from the interpreted 3-D seismic data (Krawczyk et al., 2019). The sketched model of the target horizons (c.f., Fig. 1b) shows the view of horizon shapes and their lithological architecture. All of the target horizons in the depth domain (km) and their lithological types are clearly noticeable. The S1 and X1 reflectors/horizons present the anticlinal forms which result in a thickness of ca. 800 m and the inferred almost vertical normal faults (black lines) are the result of salt mobilisation. The lithology between S1 and X1 horizons is generally alternated by marlstone and claystone. Norden et al. (2023) reported that the anhydrite (S1 lithology) is brittle compared to rock salt (X1 lithology) which is ductile. The Z1 and ERS

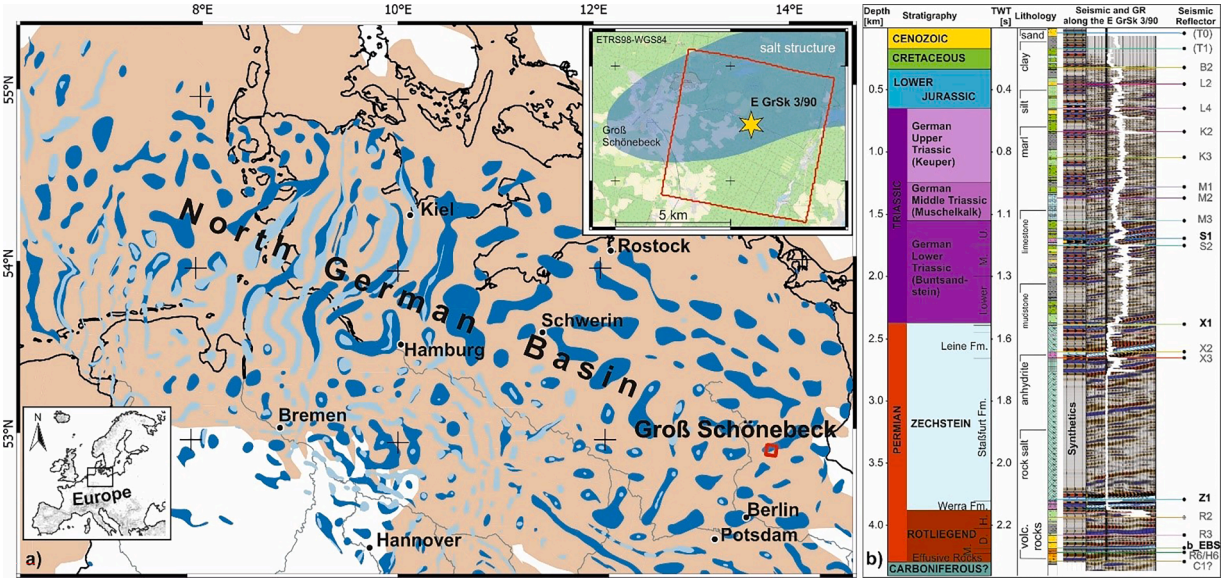


**Fig. 1.** Tectonic and geologic overview of the study area in the North German Basin around the Groß Schönebeck geothermal research platform which is located ca. 50 km north of Berlin. a) Permian (Lower Rotliegend) sediments (in brownish colours; after Dornenbal & Stevenson 2010) are shown together with the distribution of Zechstein salt structures (dark blue: salt pillow, light blue: salt diapirs; after INSpEE project data, BGR 2020). Inset shows the site of Groß Schönebeck with the area of acquired 3-D seismic data (red rectangle) and location of well E GrSk 3/90 (yellow star). b) Stratigraphic sequence of the drill hole from the Quaternary down to Rotliegend at Groß Schönebeck (after Krawczyk et al., 2019 and Norden et al., 2023). Seismic marker horizons are labelled (according to nomenclature after Reinhardt 1993), and analysed ones in this study are given in bold letters.

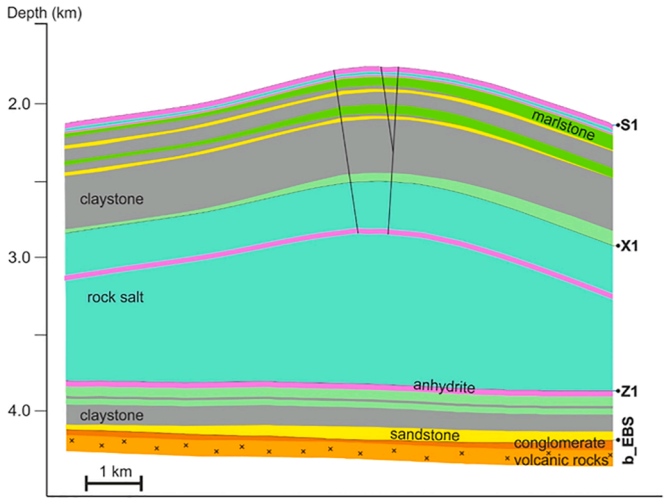


**Fig. 2.** Schematic illustration of the target horizons marked by labels (S1, X1, Z1 and b_EBS) that lie sequentially from the top to bottom. The depth of the target horizons is in km and their lithological types are indicated by colours and names. The near vertical black lines point out the inferred normal faults (Krawczyk et al., 2019; Hansen et al., 2007).

(b_EBS; base of Elbe Sandstone) horizons which are separated by around a 250 m thick layer of rock salt and claystone exhibit almost flat shapes.

## 3. Methodical background to fracture, anisotropy, and velocity analyses

Fractured rocks are one of the causes of seismic anisotropy, because they alter parameters such as travel time and wave velocity in a medium with respect to azimuthal dependence of seismic wave-propagation (Tsvankin, 2012; Vannucci, 2018).

The anisotropy of sedimentary strata is influenced by several factors. One aspect originates from grain orientation of the medium itself and isotropic layers. Their small size, if compared to the seismic wavelength, causes the intrinsic anisotropy. Another effect from near-vertical fractures or microcracks which are affected by both regional and local stresses generates the extrinsic anisotropy (e.g., Crampin, 1994; Shapiro and Kaselow, 2005; Tsvankin et al., 2012; Wang et al., 2013).

Anisotropy models based on elastic properties of the rock matrix are divided into three types of Transverse Isotropy (TI) media (Tsvankin and Grechka, 2011). Firstly, the Vertical Transverse Isotropy (VTI) model describes a sub-horizontal layering structure with fine-scale velocity alternations in vertical direction, with a symmetry axis in the vertical direction. Of importance for seismic wave propagation is that the VTI model significantly affects the seismic attributes, as for instance, travel time, amplitude, and velocity. Waves travelling perpendicular to the fine-scale velocity variations will have a reduced velocity value, while a propagation parallel to the alternating velocity structure will have a high velocity value. Secondly, the Horizontal Transverse Isotropy (HTI) model (see Fig. 3) is characterized by fine-scale velocity alternations in horizontal direction, typically caused by vertically aligned fractures with a specific, predominant azimuthal orientation. In this case, the horizontal direction is the symmetry axis. For this anisotropy model, waves travelling parallel to fracture strike are faster than for other propagation directions (Lynn et al., 1999). The difference between VTI and HTI model lies only on their symmetry axis orientation. Finally, the Tilted Transverse Isotropy (TTI) model assumes that the symmetry axis is tilted against the vertical axis.

A fractured reservoir is typically considered as an HTI medium (Gray, 2008), consisting of a single set of aligned, vertical fractures or penny-shaped cracks (parallel vertical cracks), usually caused by regional and smaller-scale tectonics (Minsley et al., 2003). Reservoirs

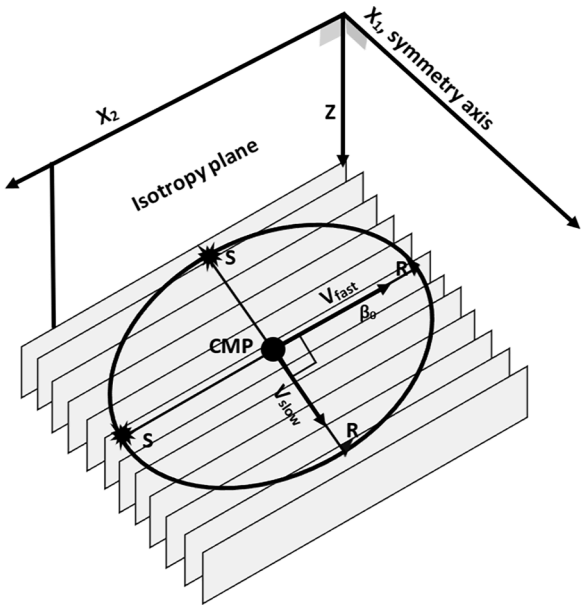


**Fig. 3.** Basic principles of analysed anisotropy of this study. The Horizontal Transversely Isotropy (HTI) model visualizes vertical fracture sets (Rüger, 1998). Source-receiver (S-R) pairs and Common Midpoint (CMP) are located relative to the symmetry axes ($X_1$). The fast velocity ($V_{fast}$) with its orientation ($\beta_0$) and the slow velocity ($V_{slow}$) perpendicular to it form the normal moveout (NMO) ellipse.

with vertical aligned fractures have been studied worldwide using the HTI model (e.g., Jenner et al., 2002, Hall and Kendall, 2003; Grechka et al., 2006; Liu, 2014) to investigate anisotropy.

In the study presented here, we use the HTI model as reference to determine azimuthal velocity anisotropy. The most common explanation for azimuthal velocity anisotropy is the presence of sub-vertical fracturing which runs parallel in a predominant azimuth direction over larger areas (see detail in Tsvankin, 1997 and Treadgold et al., 2008).

In seismic data processing, the velocity analysis makes use of the normal moveout (NMO) from hyperbolic events in Common Midpoint (CMP) data based on different source-receiver offsets. The objective of this type of velocity analysis is to flatten the hyperbola associated with a reflection into a straight horizontal event. Therefore, the velocity that produces the best alignment of stacking the multi-fold CMP traces is considered the best-fit velocity (Yilmaz, 2001; Upadhyay, 2013). In terms of assessing fractured reservoirs, the approach of Velocity Variation with Azimuth (VVA) analyses the velocity variance of P-waves in azimuthal sectors (Tsvankin and Grechka, 2011; Liu and Martinez, 2012). The basic assumption here is that P-wave velocities can be fast ($V_{fast}$) or slow ($V_{slow}$), depending on their propagation direction either parallel or perpendicular to fracture direction, respectively.

Referring to Grechka & Tsvankin (1998) the non-converted mode of reflection moveout for the P-wave's travel time dependence with respect to azimuth is formulated in equation Eq. (1):

$$\frac{1}{V_{nmo}^2(\beta)} = \frac{1}{V_{slow}^2} cos^2(\beta - \beta_0) + \frac{1}{V_{fast}^2} sin^2(\beta - \beta_0) \quad (1)$$

where $V_{nmo}(\beta)$ is the azimuthally dependant velocity with respect to the source-receiver azimuth $\beta$, $\beta_0$ is the azimuth of $V_{fast}$ (parallel to fracture), and $V_{slow}$ describes the P-wave velocity perpendicular to fracture. Fast and slow velocity form as the normal moveout ellipse and they are orthogonal each other (Fig. 3; $X_1$ and $X_2$ axes). Fig. 3 shows the basic principle of the anisotropy analysis for the HTI model. $X_1$ and $X_2$ are the symmetry axis (perpendicular to fractures) and the isotropy axis (parallel to fractures), respectively, while the vertical Z axis and the

horizontal $X_2$ axis constitute the isotropy plane. S and R are the source-receiver pairs that form Common Midpoint (CMP) at their half distances.

The determination of $V_{fast}$ and $V_{slow}$ (Grechka and Tsvankin, 1998; 1999a) is based on Eq. (2):

$$\frac{1}{V^2_{nmo}(\beta)} = W_{11}cos^2(\beta) + 2W_{12}cos(\beta)sin(\beta) + W_{22}sin^2(\beta) \quad (2)$$

where $W_{11}$, $W_{12}$, $W_{22}$ denote the gradient ellipses in orthorhombic media. The velocity analysis results in the root-mean-square velocity ($V_{rms}$) that has a close relationship to the normal-moveout velocity $V_{nmo}$ and is often conceptually approached (Yilmaz, 2001).

The interval velocity ($V_{int}$) can be derived from $V_{rms}$ using the Dix equation, that was re-arranged by Tsvankin & Grechka (2011) in Eq. (3):

$$\left[V^{(n)}_{int}\right]^2 = \frac{V^2_{nmo(n)}.T_{0(n)} - V^2_{nmo(n-1)}.T_{0(n-1)}}{T_{0(n)} - T_{0(n-1)}} \quad (3)$$

where $V_{int}$ is the interval velocity, $T_0$ is the twt at zero offset, and n is the n-th horizon.

To observe seismic anisotropy it is most reasonable to use the interval velocity rather than $V_{rms}$ because the interval velocity reflects the anisotropy of the layer instead of providing a velocity from a surface down to a horizon (Alkhalifah and Tsvankin, 1995; Tsvankin and Grechka, 2011).

To reformulate Eq. (2) in order to compute the azimuth of $V_{fast}$, we introduce Eq. (4) (Grechka and Tsvankin., 1999a, b; Jenner et al., 2002):

$$(\beta_0) = arctan\left\{\frac{W_{22} - W_{11} + \sqrt{(W_{22} - W_{11})^2 + 4W^2_{12}}}{2W_{12}}\right\} \quad (4)$$

In addition to the azimuth direction of anisotropy (parameter $\beta_0$), the other important parameter of anisotropy analysis is the magnitude of azimuthal velocity anisotropy interpreted as fracture intensity (Rüger, 1998). In the context of geothermal exploration, high values of fracture intensity indicate a potentially higher permeability if the fractures are open. For parallel vertical cracks embedded in an isotropic matrix (c.f., Fig. 3), transversely isotropic media with a horizontal axis of symmetry (HTI media) are generally chosen as model. In order to determine anisotropy magnitude in TI media, it is more applicable to utilize three unitless anisotropy notations ε, δ, and γ proposed by Thomsen (1986). Hence, Rüger (1998) uses the Thomsen parameters in the anisotropy analysis of fractured reservoirs. In our study we make use of parameter ε:

$$\varepsilon = \frac{c_{11} - c_{33}}{2c_{33}} \quad (5)$$

The notation of $c_{11}$ and $c_{33}$ is equivalent to $V_{fast}$ and $V_{slow}$, respectively. This parameter is a measure for the anisotropy magnitude which is approximately proportional to the fracture intensity (Berryman, 2009).

## 4. Database and workflow for anisotropy analysis

The data used in this study is the 3-D reflection seismic volume at Groß Schönebeck (Krawczyk et al., 2019). The controlled-source 3-D seismic measurements cover an 8 km x 8 km large survey area (Fig. 4a) which was designed to study geothermal targets below the Zechstein salt in more than 4 km depth. Data acquisition comprised 409 inlines (IL) and 399 crosslines (XL) whose Source Line Interval (SLI) and Receiver Line Interval (RLI) are 700 m and 400 m, respectively (Fig. 4). The source and receiver lines were arranged by placing the source and receiver positions at 50 m distance. This layout specifically produced the 25 m x 25 m size of Common Midpoint (CMP) bins of variable trace fold, ranging from 60 traces, at the outer areas, to about 100 traces at the centre of the survey (Stiller et al., 2018). These geometric parameters of the measurement yield the methodically required wide azimuth-offset coverage for fracture characterization (Craft et al., 1997; Ji-feng et al., 2018).

The data used were already processed with 3-D seismic data processing tools, such as static, spherical divergence, and amplitude correction then followed by deconvolution, residual statics correction, and denoising (see details in Krawczyk et al., 2019). This dataset provides the basis for picking the target horizons, and for the fault interpretation (Norden et al., 2023).

In addition to this, we introduce here the supplementary azimuth-dependant velocity analysis which makes use of the prestack 3-D seismic reflection data that is un-NMO corrected and stacked zero-phase, respectively. The 3-D un-NMOed data is used to perform velocity analysis, where the NMOed stacked zerophase is utilized to pick target horizons and fault interpretation as a comparison.

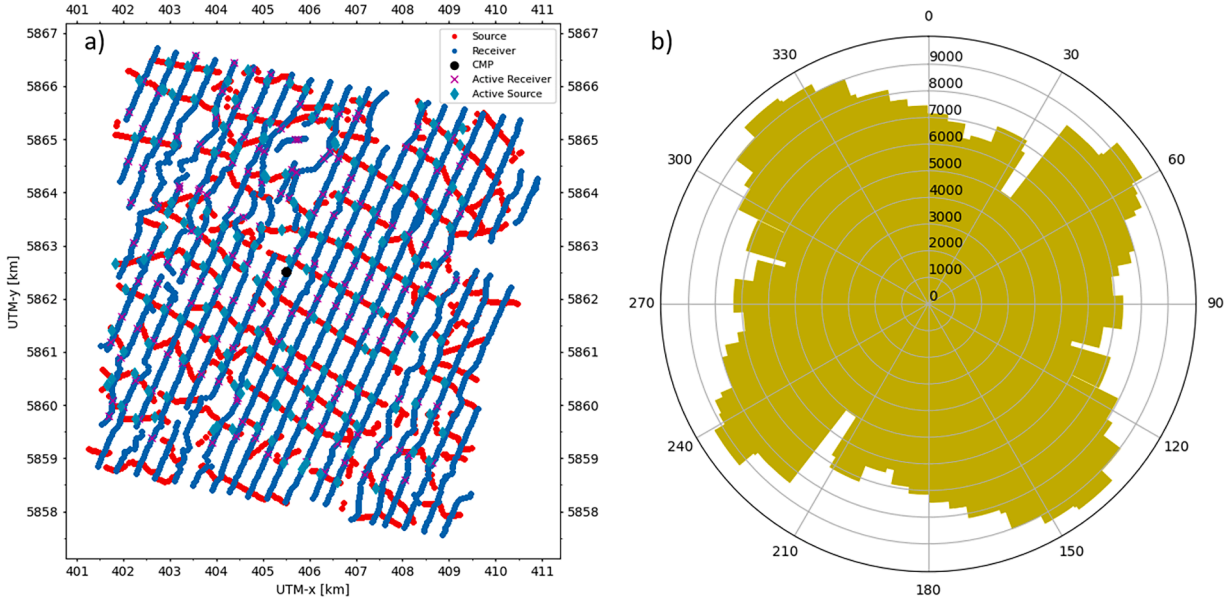


**Fig. 4.** Geometry of data used in the presented study. a) Acquisition scheme of 3-D reflection seismic survey (black filled circle marks CMP 77,398 exemplified in b). b) Azimuthal offset distribution (30°-segments labelled) of CMP 77,398 that is located close to the centre of the research area and extracted from Inline 10,391 and Crossline 2381. The offset length (metre) runs from 0 to 9000 m, the zero coincides with the CMP position.

The first step in the workflow is to read and convert the Groß Schönebeck SEGY data to Python including inline (IL) and CMP information (Fig. 5), because ProMax does not have a tool to perform azimuth division.

Secondly, we evaluate the azimuth-offset distribution for all data (according to the example given in Fig. 4). The evaluation step is sorting rich offset-azimuth coverage to fulfil the requirement of fracture delineation for target horizons.

The third step is dividing the full azimuth data into six azimuthal sectors, encompassing 30° each, for subsequent azimuthal velocity analysis. This aims to provide the spatial fracture characteristics in more detail and results in localized information. To evaluate the quality of the data and to enhance the robustness of horizon picking, five neighbouring CMPs were combined to a central CMP for maximum coherence, and the semblance-velocity spectra displayed (Fig. 6). The example spectra extracted for CMP 77,398 in the middle of the study area (compare Fig. 3) reveal that the semblance maxima correlate well with the expected depths of the target horizons in the area (see horizons S1, X1, Z1, and ESR in Figs. 1, 2 and 6). Apparently, the panels with azimuths of 0–90° exhibit a strong signal for the shallower subsurface (panels b-d in Fig. 6; upper 1.5 s twt), while azimuths within the range of 90 to 180° show a strong signal at larger depth (panels e-g in Fig. 6; 1.5–3 s twt). Because of the multi-fold survey character and data redundancy, such weaker azimuthal sectors are easily compensated by other CMPs, resulting in robust velocity analyses.

The fourth step is to re-convert the Python based CMP.py files to SEGY as input for the ProMax software. The following stage is to perform velocity analyses on each azimuth from sector 1 to sector 6. In parallel to the velocity analyses, the target horizons are picked. This enables us to interactively compare the horizons from different pickings. Both picks result in a velocity profile versus two-way-traveltime (twt) and twt of the horizon outlooks. As shown in Fig. 6, the semblance spectra show a good quality coherence which leads to a confident picking for flattening azimuthal gathers in advance. At this stage, we also calculate the interval velocities for all sectors and the target horizons in sequential way. The computation of the interval velocity is performed after fitting the picked travel time (twt) to a horizon (using the Petrel software), and the travel time to this horizon is derived from the velocity analysis of every CDP. This ensures that the time slices from two different approaches picking the same horizon actually match. The interval velocity is finally calculated by using Eq. (3). Layer means that we consider the target horizon as the top of the layer, and add 20 ms of the seismic volume below it, so that a layer thickness is assigned and we can work with interval velocities.

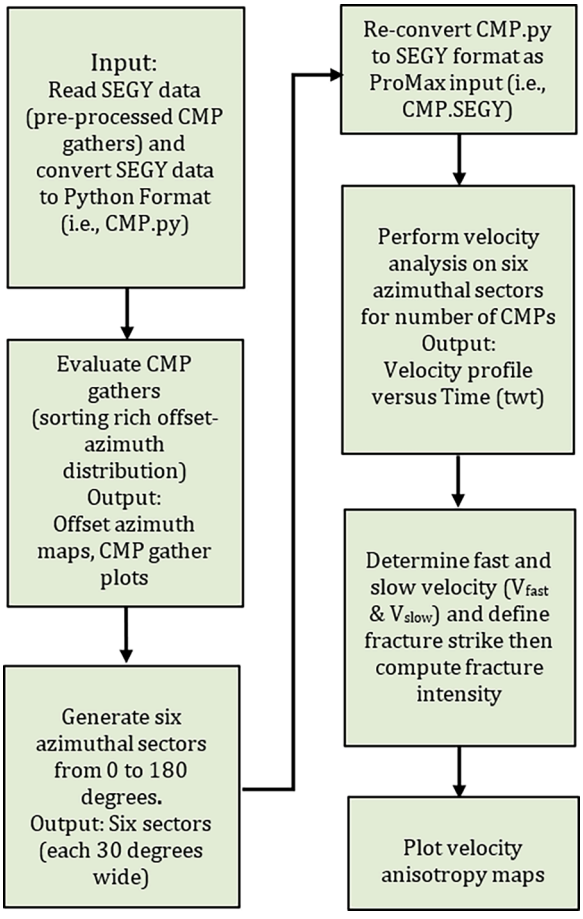


**Fig. 5.** Workflow for anisotropy analysis used in this study.

The pre-final step in the workflow Fig. 5) is to determine the $V_{fast}$ and $V_{slow}$ values for every CDP in each layer and all six azimuth sectors in which azimuths exist. From this result, the azimuthal fast velocity is assigned as the fracture strike, where the fractional difference between $V_{fast}$ and $V_{slow}$ divided by 2 times of $V_{slow}$ is stated as the anisotropy magnitude or an approximation to the fracture intensity. The calculation of these two fracture characteristics are based on the Eqs. (4) and ((5) respectively. Finally, the anisotropy maps are plotted as the end product and interpreted in the overall geological context.

The anisotropy phenomenon could also be observed through the Common Offset Common Azimuth (COCA). The COCA is also useful for the analysis of azimuthally dependant seismic attributes. It is a sorted offset and azimuth of the NMO gather. Therefore, azimuthal gathers after NMO has been applied, provided a snail pattern expressing the anisotropy signatures if they exist at subsurface horizons (Li, 2008).

The first outcome of the anisotropy analysis is that the azimuthal COCA gathers tested for the GrSk dataset show the anisotropy signature of the target horizons from only one CDP (Fig. 7). Fig. 7a shows the COCA gather before the trace interpolation was performed. It is noteworthy that empty traces are present before the interpolation is carried out and this results in an unclear snail gather at the horizons because of discontinuing events. However, after employing an interpolation (Fig. 7b), the snail gathers are moderately apparent as shown in the zoomed-in black boxes. There is only the Z1 horizon, where the anisotropy is not clearly apparent, but the S1, X1, and ERS horizons show the snail gather moderately. For the Mesozoic horizon S1, the anisotropy is present at the offset range of 2047–2200 m and in the azimuth range of 150–180°. This result suggests to carry out a further assessment of the anisotropy to the target horizons, and its results are presented in Section 5.

## 5. Deduced horizon characteristics

With the method explained above, we analysed in total four horizons, one representing Mesozoic strata (above the Permian Zechstein salt, S1) and three representing Palaeozoic strata (Permian Zechstein salt and below: X1, Z1, ERS). Similar to other comparable studies (e.g., Hall and Kendall, 2003; Zhang et al., 2020) we assume that natural sub-vertical fracturing is the main source of the observed azimuthal anisotropy.

Figs. 8 and 9 show the time and the velocity anisotropy maps of the studied horizons. The time maps of the Mesozoic horizon (S1) and those above the Permian Zechstein salt (X1) show a very similar pattern (Fig. 8a and b), recapturing the structure and geometry of the underlying salt pillow. The anticlinal structure is SSW-NNE orientated and shows a maximum rise north of the Groß Schönebeck (GrSk) drill sites. The corresponding velocity anisotropy maps (Fig. 8c and d) exhibit, however, different patterns for the two horizons. For the Mesozoic horizon S1, a distinct change of the velocity anisotropy is observed within the mapped fault system at the top of the salt structure (Fig. 8c). The magnitude of anisotropy amounts to about 0.1, which is higher than the values < 0.03 that are observed in the adjacent areas towards the south,

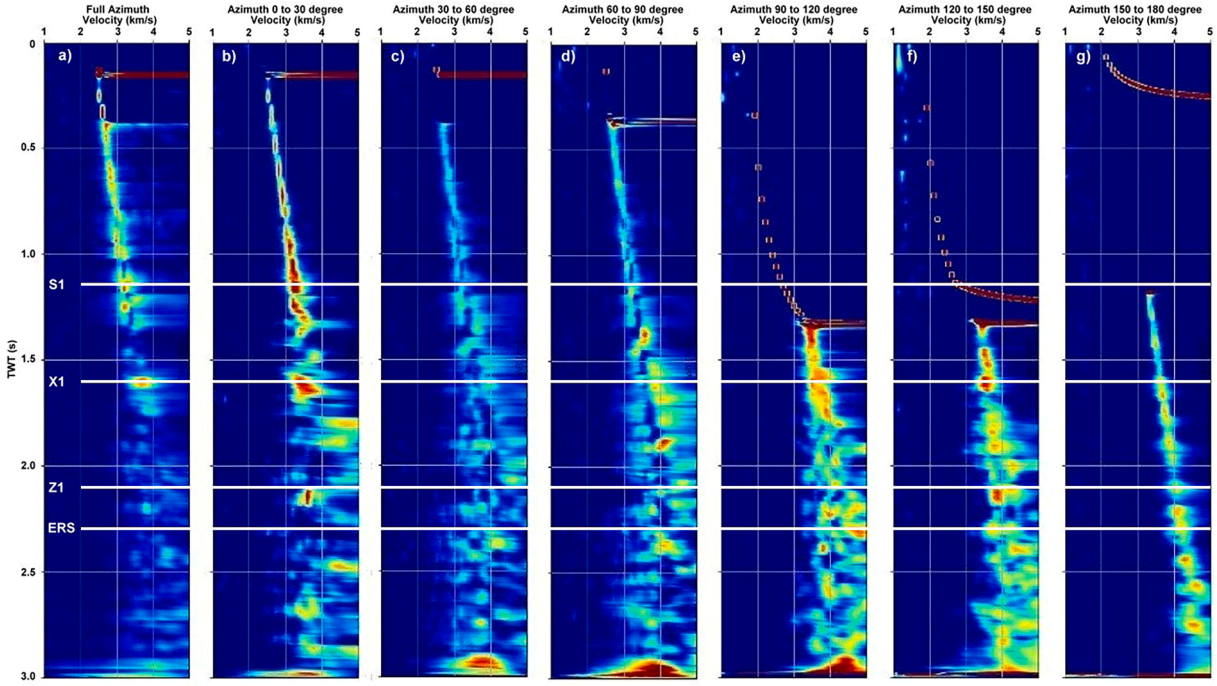


**Fig. 6.** Semblance velocity spectra for CMP 77,398 (c.f., Fig. 4) between 0 and 3 s twt. The panels for full azimuth and six azimuthal sectors (0–180° with 30° increment; a-g show azimuthal semblance maxima for the target horizons (labelled with white colour capital letters S1, X1, Z1, and ERS (b_EBS) and lines; see also Figs. 1, 2).

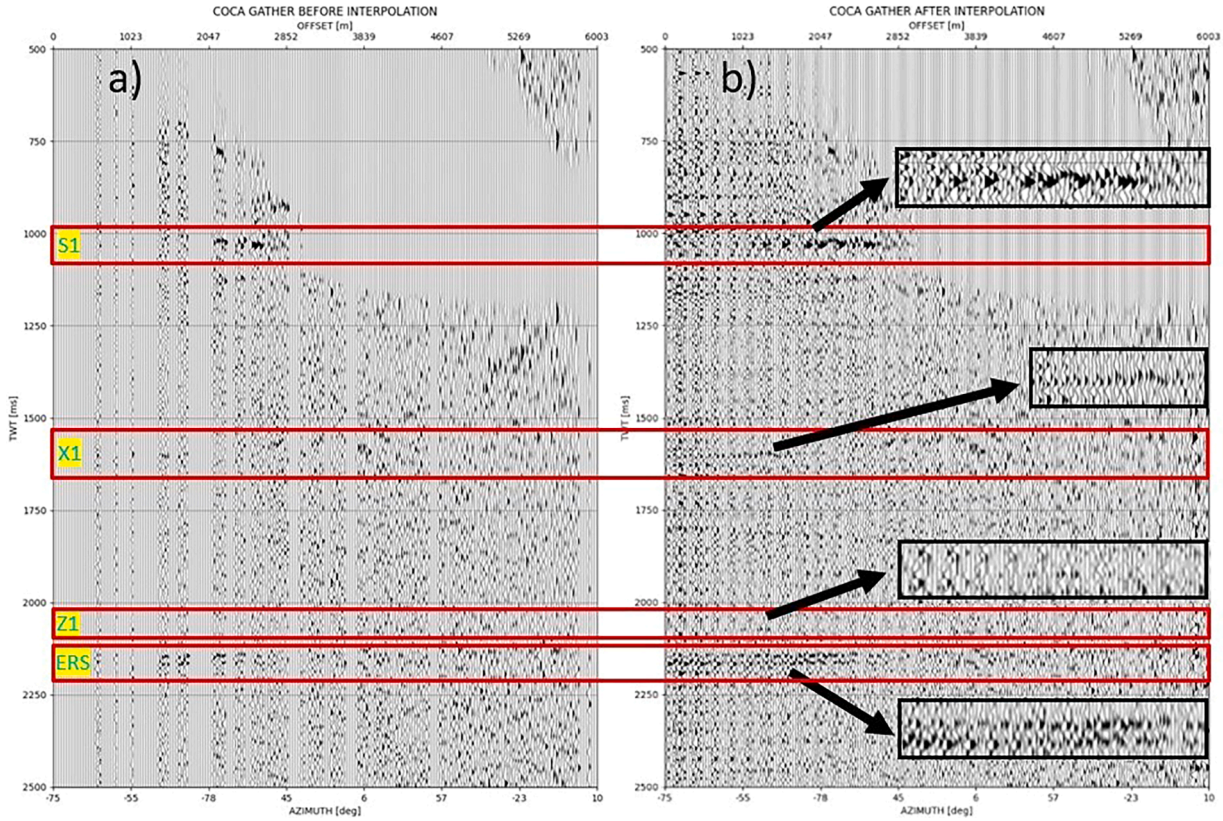


**Fig. 7. .** Common Offset Common Azimuth (COCA) gathers a) before and b) after trace interpolation. The four analysed horizons are shown in the red rectangle boxes, where the detailed views of the variable anisotropy signatures of the four analysed horizons (S1, X1, Z1, and ERS) are highlighted in the black rectangle boxes.

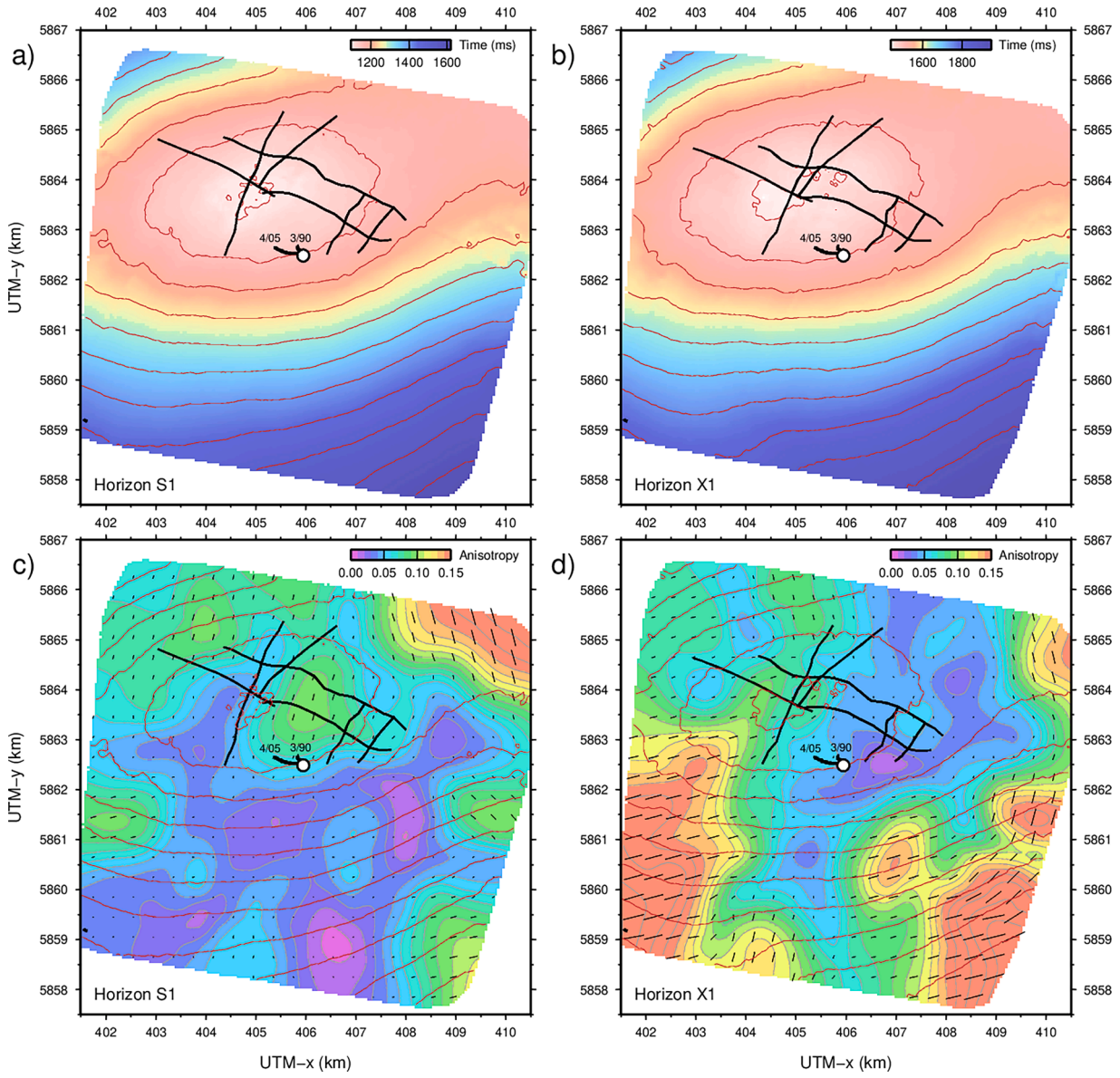


**Fig. 8.** Analysis of horizon S1 (within Upper Buntsandstein; subfigures a, c) and of the horizon X1 (top of Permian Zechstein, subfigures b, d) showing the colour-coded two-way travel time (a, b) and the magnitude of anisotropy (parameter ε) and inferred fracture orientation (black lines, the length of the line correlates to the magnitude of anisotropy; c, d). The colour-coded travel time map is additionally contoured in 50 ms intervals that are also projected onto the velocity anisotropy maps. Superimposed are the mapped fault system at the top of Zechstein after Norden et al., 2023 (bold black lines) and the positioning of the Groß Schönebeck Pilot Site (white circle) with the drill paths to the final depths of the E GrSk 3/90 and Gt GrkSk 4/05 wells (solid black).

west and east. The fracture orientation estimated by the applied method shows a very consistent orientation of ca.15° to the north for this area. In physical terms, this area represents a zone where the enclosed rocks show a faster velocity of waves in the north direction compared to the west-east direction. Lower anisotropy values do prevail for large regions south of the Groß Schönebeck drill sites (i.e. on most of the structural flanks), higher values are observed north of the drill sites, at the top of the salt pillow, again. Another region with a higher degree of anisotropy is located in the NE (around the top-right corner of the research area). This area exhibits the maximum values of anisotropy for this layer. Due to the low data coverage at the marginal position, we will not discuss this feature in more detail.

Compared to the anisotropy orientation determined for the S1 horizon, the orientation for the X1 layer (Fig. 8d) is shifted to the northwest, and the fracture orientations are rotated clockwise and amount to ca. 75° N. The anisotropy pattern of X1 south of the GrSk drill sites is similar to the pattern of the analysed S1 horizon, but in general shows a higher magnitude of anisotropy. The smaller-scaled anomaly around the coordinate 406.5/5860.5 shows a value of about 0.14 and a fracture orientation of ca. 75° N. The lowest anisotropy values of the X1 horizon are found north and east of the drill sites, showing no distinct fracture orientation. While the magnitude of velocity anisotropy is different between the two layers, the fracture orientation correlates quite often, except for an area in the central eastern margin (coordinate 409.7/5861.5).

For the horizon at the base of the Permian Zechstein salt (Z1) and for the Rotliegend ERS horizon, the two-way travel time structure patterns look quite similar (Fig. 9a, b). The horizons are relatively flat, covering a range of about 200 ms between minimum and maximum two-way travel time. In contrast, the corresponding velocity anisotropy maps for the two marker horizons (Fig. 9c, d) look different. The analysis of the velocity anisotropy of Z1 (Fig. 9c) shows a trend towards lower magnitudes (especially in the vicinity of the wells) compared to the Mesozoic S1 horizon (Fig. 8c), whereas in this layer the moderate anisotropy is

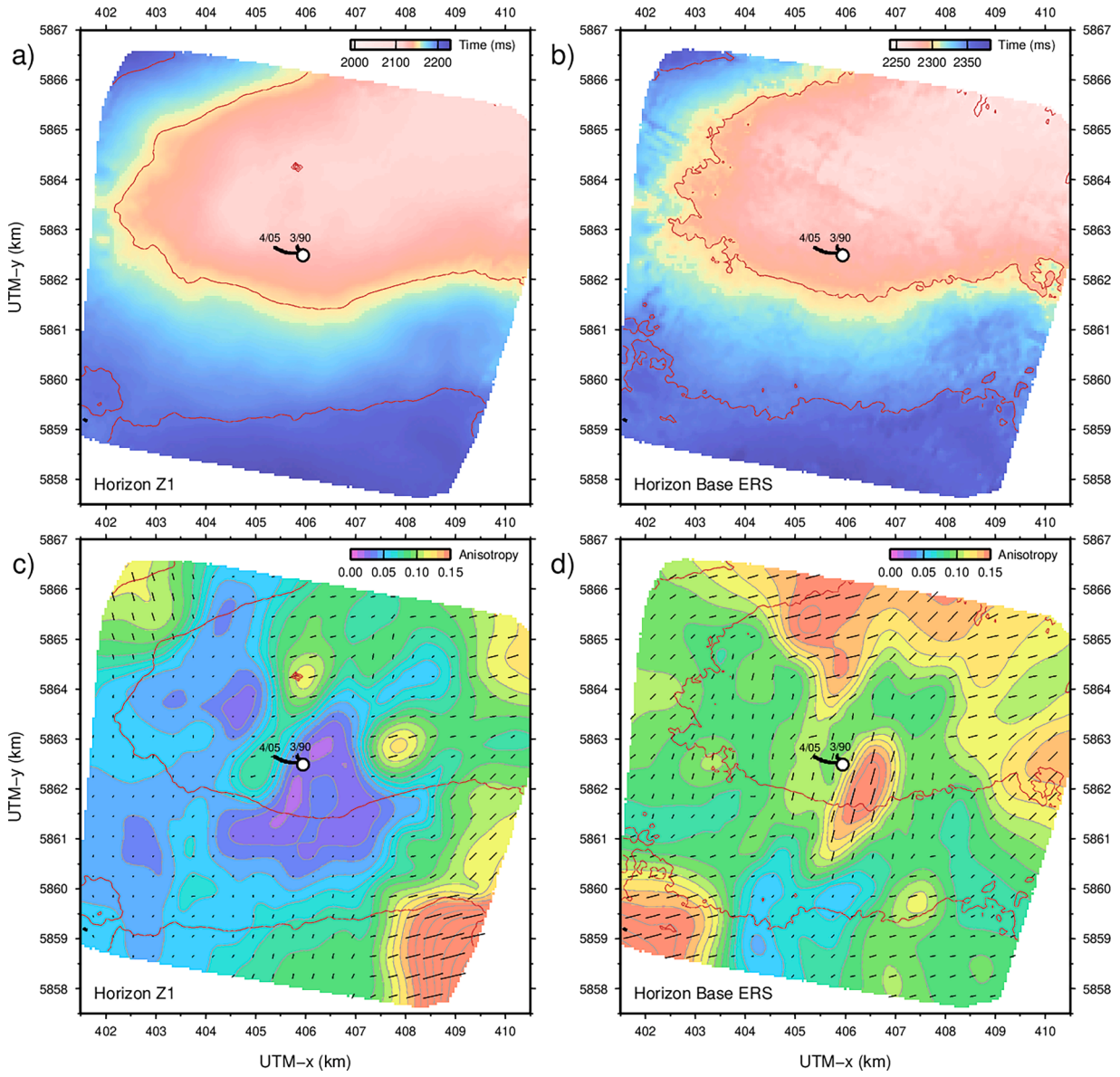


**Fig. 9.** Analysis of Z1 horizon (at the base of Permian Zechstein; subfigures a, c) and of the ERS horizon (within Dethlingen Formation, subfigures b, d) showing the colour-coded two-way travel time (a, b) and the magnitude of anisotropy (parameter ε) and inferred fracture orientation (black lines, the length of the line correlates to the magnitude of anisotropy; c, d). The colour-coded travel time map is additionally contoured according to the range of the colour bar, and also projected onto the velocity anisotropy maps. Superimposed is the positioning of the Groß Schönebeck Pilot Site (white circle) with the drill paths of the E GrSk 3/90 and Gt GrkSk 4/05 wells (solid black). From the 3-D seismic, no faults were mapped for these horizons.

separated by the lowest degree anisotropy areas. This weak anomaly has a fracture orientation of ca. 75° N in the south and north-eastern regions. Zones with a higher degree of anisotropy are found in the north and east of the well spots. Those anomalies have a fracture orientation of ca. 75° N.

The ERS horizon (Fig. 9b) is flatter than the Z1 horizon (Fig. 9a), indicated by a-100 ms difference of minimum and maximum twt (see the interval scale), and the highest values of anisotropy are found close to the drill sites (Fig. 9d). This anomaly has a fracture orientation of ca.15° N. Another anomaly with high anisotropy values is located in the north of the well locations and indicates predominant fracture orientations of around 75° N.

## 6. Discussion and interpretation

The appropriateness of anisotropic models applied on seismic subsurface data depends on the characteristics of the respective geological setting. For example, anisotropy could be caused by near vertical fractures (Rüger, 1997 and references therein) and by fine-layered and dipping shale, or by overthrust belts which tilt more than 30° (Behera, 2022). Based on the respective geological setting, an adequate anisotropy model should be used. For observing the azimuthal anisotropy, the HTI model serves best. For fine-layered strata, the VTI model is preferred while for thrust belt settings, the TTI model is recommended (Behera, 2022). We decided to use the HTI model because based on the observed fault pattern, a near-vertical fracture (normal faulting) regime appears reasonable. Areas showing a high anisotropy will represent zones of a high fracture swarm density, and thus highlight possible exploration targets that may exhibit good fracture permeability. Compared to other methods, using seismic amplitude and frequency data is not a robust method due to unsolved acquisition footprints and it would require perfect true amplitude processing. In contrast, the azimuthal velocity analysis is a robust method which is not so sensitive to the data quality (noise to signal ratio) and it is taking advantage of the many trace fold

data and the rich offset azimuth coverage. The HTI model could be further improved by the integration of additional data, e.g., if any structural borehole data were available, ambiguous HTI patterns could be interpreted and cross-checked. Additionally, an inversion of anisotropy parameters could be performed and compared to the HTI anisotropy model. Future work may also consider a combination with the Amplitude Variation with Azimuth (AVA) approach.

In our study, we have chosen well-pronounced, traceable seismic horizons and applied the HTI approach, considering strata above and below the Permian Zechstein, to provide some first insights into possible fracture network orientations for an initial structural characterization of potential geothermal targets (e.g., within the Buntsandstein or the sedimentary Rotliegend). It was expected that the horizons will cover different stress-field regimes (Marotta et al., 2001), as the Zechstein salt decouples the stress field between the subsalinar and the suprasalinar (see, e.g., Röckel and Lempp, 2003). Hence, we evaluated if this assumed difference of stress-field is reflected in different anisotropy patterns above and below the Zechstein salt succession.

### 6.1. Top salt and Supra-Salinar pattern (S1 and X1 horizons)

The moderate magnitude of anisotropy (north of drill sites) for the uppermost studied horizon (S1, Fig. 8c) can be linked to seismically mapped faults in the anticlinal top. The fault system consists of NNE-SSW and NE-SW orientated faults that intersect with NW-SE orientated faults. The orientation of the moderate anisotropy anomaly seems to follow the NE-SW fault structure orientations (see Fig. 8c). The faults mapped from the 3-D volume by Norden et al. (2023) were interpreted to originate from the salt doming process, producing normal faults. Based on the 3-D seismic data, fault offsets are expected to be small. Such systems are known from Hansen et al. (2007) for the upper Buntsandstein forming fracture swarms. In contrast, the two parallel NW-SE orientated faults are more or less perpendicular to the velocity anomaly orientation. The faults are interpreted as a graben structure (Bauer et al., 2010; Norden et al., 2023), and the anomaly does not follow the graben trend because the moderate anisotropy is seemingly controlled by the NNE-SSW and NE-SW faults patterns. Unfortunately, no structural logs or other data is provided by any drilling in that area.

The analysed horizon correlated with the X1 horizon (Fig. 8d), shows a different velocity anisotropy pattern than the S1 horizon. Whereas one part of the observed anisotropy anomaly at the top of the anticlinal structure is still in some agreements with the NE-SW orientated faults (right beside the NNE-SSW fault), this is not the case for other parts. The anisotropy distribution of layer X1 physically represents the structural setting at the top of the Zechstein salt structure. According to the distribution of higher anisotropy magnitudes from southeast to northwest, the pattern can be inferred as a footprint of salt motion, where the length of the slope/flank of the southeastern side is longer than of the northwestern side (see also Krawczyk et al., 2019, in Fig. 5b), causing variable fracture directions. These various strikes are to be expected geo-dynamically due to the process in the up-doming salt structure experiencing two stages which are up and down (Norden et al., 2023). On the other hand, the highest anisotropy magnitude, forming such a counter clockwise trend of fracture orientation, is probably affected by salt mobilization that ended at the vicinity northwest of the well sites forming the salt anticline. As a general trend along horizon X1, the largest anisotropy values are observed in the outer parts of the updoming salt pillow, where the top of the Zechstein runs deeper and the thickness of the salt layer is decreasing (Fig. 8b,d; Norden et al., 2023). A seismic tomography study of Bauer et al. (2010) revealed systematic velocity variations within the Zechstein layer. Higher velocities in salt lows compared with lower velocities in the up-doming salt pillows were interpreted as the remaining denser components of the mobilized salt. Such denser, and, hence, more brittle salt rocks could be responsible for the increased anisotropy and interpreted fracturing in the outer regions of the salt pillow.

### 6.2. Base and below Zechstein (sub-salinar) horizons (Z1 and ERS)

The anisotropy analysis of velocity for the Z1 horizon comprises larger areas of lowest anisotropy magnitude (Fig. 9c). The anisotropy orientation in those areas as well as in the areas of more moderate anisotropy magnitudes may be influenced by short-scale effects. From seismic analysis of the 3-D seismic volume, no distinct fault patterns were mapped in this depth interval. Kossow et al. (2000) and Scheck et al. (2003) report similar observations for the base of the Zechstein salt, concluding that faults, if present in that depth level, are of minor offsets showing lengths below seismic resolution.

Therefore, the overall trend of anisotropy magnitude in this layer should be fairly consistent. For the layer associated with the ERS horizon, the high-magnitude anomaly of anisotropy east of the GrSk 3/90 borehole is a dominant feature (Fig. 9d). The observed fracture orientation is roughly in agreement with the expected orientation of the maximum horizontal stress, which was determined for the sedimentary Rotliegend by borehole imaging of artificially induced fractures in the GrSk 3/90 borehole to amount to 18.5° N (Moeck et al., 2009a). For the sub-salinar, other studies show similar stress field orientations (e.g., Roth et al., 1997; Marotta et al., 2001; 2002, and World Stress Map, 2000).

The higher magnitudes of anisotropy in the north of the well sites may originate from fractures around a system of paleo-channels that were derived from a 3-D seismic analysis of seismic attributes (Bauer et al., 2020). This may also cause the prominent anisotropy magnitude (green colour) in the northeast.

In contrast to the other investigated layers in this study, the dominant rock type in the ERS layer is sandstone. Sandstone is less susceptible to stress-induced fracture, because it is in general more porous. Therefore, the anisotropy in this layer is less pronounced compared with the other three investigated layers. The variability of anisotropy (fracture) orientation may also be affected by lithological changes due to variations of the depositional system (McCann, 1998; Norden et al., 2023).

## 7. Conclusion

Our velocity anisotropy analysis represents a first attempt to use this method for geothermal reservoir characterization and future site development. In particular, the study faced some challenges which are related to site-specific characteristics, such as the limited number of boreholes and the lack of detailed information on existing fractures based on the structural data. The observed heterogeneity of velocity anisotropy within the different horizons also reflects a natural lithological heterogeneity leading to different fracture behaviour or to local fracture cementation, overprinting the fracture signature in the seismic velocity analysis. If more data were available, i.e. cores and borehole structural imaging tools, a direct comparison of the result or an inversion approach could be performed and compared to our velocity anisotropy analysis.

We conclude that for the horizons above the Zechstein salt, such as the Mesozoic S1 horizon, the interesting anisotropy anomalies are located in the vicinity north of the drill sites which have a consistent fracture orientation of ca. 15° N, fairly agreeing with the NNE-SSW and NE-SW faults mapped by the 3-D seismic. The pronounced magnitude anisotropy of the uppermost Permian X1 horizon in the northwestern area of the well sites which show variable fracture orientation also seems to be partly controlled by the NE-SW fault. The detection of larger anisotropy anomalies above the salt structure may justify to study the geothermal potential of possible Mesozoic reservoirs. Due to a normal faulting regime which is expected at the top of the salt anticline, even reservoirs with lower thicknesses may allow sufficient fluid production, if the faults are still permeable. The higher productivity would compensate for the lower temperatures that have to be expected at shallower depths.

The deeper horizons below the Zechstein show a different anisotropy

distribution pattern. The Permian Z1 horizon (base Zechstein) exhibits no traceable faults. The observed anisotropy anomaly trends show variable fracture orientations mostly from north to south with a clockwise pattern. For the analysed ERS horizon, higher anisotropy values magnitudes are present in the area east of well sites, well corresponding to the orientation of the determined stress field showing an orientation of 18.5° N.

For future geothermal exploration and exploitation of the Groß Schönebeck site, horizons above the top of the Zechstein structure should be considered in more detail. The velocity anomalies found may result from a more intense fracturing in an extensional setting, which will additionally build up flow paths, create secondary permeability and thus enhance the fluid productivity by assessing larger rock volumes.

Our results present a first understanding of the fracture characteristics below and above the Permian Zechstein salt in and around Groß Schönebeck area. When new explorational data will become available, the robustness of the method can be better evaluated and be used to verify the findings of this study.

## Credit authorship contribution statement

**Asrillah Asrillah:** Conceptualization, Methodology, Data curation, Data analysis, Visualization, Interpretation, Writing – original draft, Writing – review & editing. **Agus Abdullah:** Methodology, Software curation, Data analysis, Writing – review & editing. **Klaus Bauer:** Supervision, Data curation, Visualization, Writing – review & editing. **Ben Norden:** Visualization, Interpretation, Writing – review & editing. **Charlotte M. Krawczyk:** Supervision, Writing – original draft, Writing – review & editing.

## Declaration of Competing Interest

The authors declare that they have no known competing financial interests or personal relationships that could have appeared to influence the work reported in this paper.

## Data availability

The authors do not have permission to share data.

## Acknowledgments

The 3-D seismic data set used in this study was generated as part of the research project RissDom-A, for which funding was provided by the German Federal Ministry for Economic Affairs and Energy (BMWi grant 0324065). The author and co-authors further acknowledge the support of the Indonesian Ministry of Education, Culture, Research and Technology (BPP-LN Scholarship T/918/D3.2/KD.02.01/2019) through the Directorate of Higher Education-Dikti Scholarship Board which fully financed the author's study and we are also grateful to Dr. Daniele Hoffmann for proofreading the manuscript.

## References

Aleardi, M., Mazzotti, A., Tognarelli, A., Ciuffi, S., Casini, M., 2015. Seismic and well log characterization of fractures for geothermal exploration in hard rocks. Geophys. J. Int. 203 (1), 270–283. https://doi.org/10.1093/gji/ggv286.

Agemar, T., Alten, J.A., Ganz, B., Kuder, J., Kühne, K., Schumacher, S., Schulz, R., 2014. The geothermal information system for Germany–GeotIS. Zeitschrift der deutschen Gesellschaft für Geowissenschaften 129–144. https://doi.org/10.1127/1860-1804/2014/0060.

Alkhalifah, T., Tsvankin, I., 1995. Velocity analysis for transversely isotropic media. Geophysics 60 (5), 1550–1566. https://doi.org/10.1190/1.1443888.

Al-Marzoug, A.M., Neves, F.A., Kim, J.J., Nebrija, E.L., 2006. P-wave anisotropy from azimuthal AVO and velocity estimates using 3D seismic data from Saudi Arabia. Geophysics 71 (2), E7–E11. https://doi.org/10.1190/1.2187724.

Bakulin, A., Grechka, V., Tsvankin, I., 2000. Estimation of fracture parameters from reflection seismic data—Part I: HTI model due to a single fracture set. Geophysics 65 (6), 1788–1802. https://doi.org/10.1190/1.1444863.

Bauer, J.F., Krumbholz, M., Meier, S., Tanner, D.C., 2017. Predictability of properties of a fractured geothermal reservoir: the opportunities and limitations of an outcrop analogue study. Geotherm. Energy 5 (1), 1–27. https://doi.org/10.1186/s40517-017-0081-0.

Bauer, K., Norden, B., Ivanova, A., Stiller, M., Krawczyk, C.M., 2020. Wavelet transform-based seismic facies classification and modelling: application to a geothermal target horizon in the NE German Basin. Geophys. Prospect. 68 (2), 466–482. https://doi.org/10.1111/1365-2478.12853.

Behera, L., 2022. Elastic anisotropic finite-difference full-wave modeling and imaging of 2D tilted transversely isotropic (TTI) media. J. Appl. Geophy. 207, 104837. https://doi.org/10.1016/j.jappgeo.2022.104837.

Berryman, J.G., 2009. Aligned vertical fractures, HTI reservoir symmetry and Thomsen seismic anisotropy parameters for polar media. Geophys. Prospect. 57 (2), 193–208. https://doi.org/10.1111/j.1365-2478.2008.00767.x.

Blöcher, G., Reinsch, T., Henninges, J., Milsch, H., Regenspurg, S., Kummerow, J., Francke, H., Kranz, S., Saadat, A., Zimmermann, G., Huenges, E., 2016. Hydraulic history and current state of the deep geothermal reservoir Groß Schönebeck. Geothermics 63, 27–43. https://doi.org/10.1016/j.geothermics.2015.07.008.

Bauer, K., Moeck, I., Norden, B., Schulze, A., Weber, M., Wirth, H., 2010. Tomographic P wave velocity and vertical velocity gradient structure across the geothermal site Groß Schönebeck (NE German Basin): relationship to lithology, salt tectonics, and thermal regime. J. Geophys. Res.: Solid Earth 115 (B8), B08312. https://doi.org/10.1029/2009JB006895.

Craft, K.L., Mallick, S., Meister, L.J., Van Dok, R., 1997. Azimuthal anisotropy analysis from P-wave seismic traveltime data. SEG Technical Program Expanded Abstracts 1997. Society of Exploration Geophysicists 1214–1217.

Crampin, S., 1994. The fracture criticality of crustal rocks. Geophys. J. Int. 118 (2), 428–438. https://doi.org/10.1111/j.1365-246X.1994.tb03974.x.

Doornenbal, H., Stevenson, A., 2010. Petroleum Geological Atlas of the Southern Permian Basin Area. EAGE.

Faulds, J., Hinz, N., 2015. Favorable tectonic and structural settings of geothermal systems in the Great Basin region, western USA: proxies for discovering blind geothermal systems. In: Proceedings World Geothermal Congress, Melbourne, Australia, 19-25 April 2015 (No. DOE-UNR-06731-02). Nevada Bureau of Mines and Geology, University of Nevada, Reno. NV 89557.

Gazar, A.H., Javaherian, A., Sabeti, 2011. Analysis of effective parameters for semblance-based coherency attributes to detect micro-faults and fractures. J. Seismic. Explor. 20, 23–44.

Garotta, R., 1989. Detection of azimuthal anisotropy. SEG Technical Program Expanded Abstracts 1989 Society of Exploration Geophysicists, pp. 861–863. https://doi.org/10.1190/1.1889795.

Grant, M., 2013. Geothermal Reservoir Engineering. Elsevier, pp. 3–4.

Gray, D., 2007. Observations of seismic anisotropy in prestack seismic data. In: 2007 SEG Annual Meeting, https://doi.org/10.1190/1.2792394.

Gray, D., 2008. Fracture detection using 3D seismic azimuthal AVO. CSEG Recorder 33 (3), 40–49.

Grechka, V., Tsvankin, I., 1998. 3-D description of normal moveout in anisotropic inhomogeneous media. Geophysics 63 (3), 1079–1092. https://doi.org/10.1190/1.1444386.

Grechka, V., Tsvankin, I., 1999a. 3-D moveout velocity analysis and parameter estimation for orthorhombic media. Geophysics 64 (3), 820–837. https://doi.org/10.1190/1.1444593.

Grechka, V., Theophanis, S., Tsvankin, I., 1999b. Joint inversion of P-and PS-waves in orthorhombic media: theory and a physical modeling study. Geophysics 64 (1), 146–161. https://doi.org/10.1190/1.1444512.

Grechka, V., Vasconcelos, I., Kachanov, M., 2006. The influence of crack shape on the effective elasticity of fractured rocks. Geophysics 71 (5), D153–D160. https://doi.org/10.1190/1.2240112.

Hall, S.A., Kendall, J.M., 2003. Fracture characterization at Valhall: application of P-wave amplitude variation with offset and azimuth (AVOA) analysis to a 3D ocean-bottom data set. Geophysics 68 (4), 1150–1160. https://doi.org/10.1190/1.1598107.

Hansen, M.B., Scheck-Wenderoth, M., Hübscher, C., Lykke-Andersen, H., Dehghani, A., Hell, B., Gajewski, D., 2007. Basin evolution of the northern part of the Northeast German Basin—insights from a 3D structural model. Tectonophysics 437 (1–4), 1–16. https://doi.org/10.1016/j.tecto.2007.01.010.

Holl, H.-G., Moeck, I., Schandelmeier, H., 2005. Characterisation of the tectono-sedimentary evolution of a geothermal reservoir – implications for exploitation (Southern Permian Basin, NE Germany). In: Proceedings World Geothermal Congress 2005, Antalya, Turkey, 24-29 April 2005, pp. 1–5.geothermal-energy.org.

Hoth, K., Rusbült, J., Zagora, K., Beer, H., Hartmann, O., Schretzenmayr, S., 1993. Die tiefen Bohrungen im Zentralabschnitt der Mitteleuropäischen Senke: dokumentation für den Zeitabschnitt 1962-1990, Schriftenreihe für Geowissenschaften. Verl. d. Ges. f. Geowiss. 145. Berlin.

Jenner, E., Williams, M., Davis, T., 2001. A new method for azimuthal velocity analysis and application to a 3D survey, Weyburn field, Saskatchewan, Canada. SEG Technical Program Expanded Abstracts 2001. Society of Exploration Geophysicists 102–105. https://doi.org/10.1190/1.1816256.

Jenner, E., 2002. Azimuthal AVO: methodology and data examples. The Leading Edge 21 (8), 782–786. https://doi.org/10.1190/1.1503184.

Ji-feng, D., Yi, B., Jia-yi, W., Jiang-yun, P., 2018. OVT domain regularization technique application in Wide-azimuth, Broadband and High-density seismic data processing. In: International Geophysical Conference, Beijing, China, 24-27 April 2018. Society

of Exploration Geophysicists and Chinese Petroleum Society, pp. 286–288.https://doi.org/10.1190/IGC2018-070.
Kossow, D., Krawczyk, C., McCann, T., Strecker, M., Negendank, J.F., 2000. Style and evolution of salt pillows and related structures in the northern part of the Northeast German Basin. Int. J. Earth Sci. 89 (3), 652–664. https://doi.org/10.1007/s005310000116.
Krawczyk, C.M., McCann, T., Cocks, L.R.M., England, R., McBride, J., Wybraniez, S., McCann, T., 2008a. Caledonian tectonics. In: The Geology of Central Europe, 1. Geological Society, London, pp. 301–381. ISBNprint: 978-1-86239-245-8.
Krawczyk, C.M., Rabbel, W., Willert, S., Hese, F., Götze, H.-J., Gajewski, D., SPP-Geophysics Group., 2008b. Crustal structures and properties in the Central European Basin system from geophysical evidence. In: Littke, R., Bayer, U., Gajewski, D., Nelskamp, S. (Eds.), Dynamics of Complex Intracontinental Basins: The Central European Basin System. Springer Verlag, Heidelberg, pp. 67–95. ISBNprint: 978-3-540-85084-7.
Krawczyk, C.M., Tanner, D.C., Henk, A., Trappe, H., Ziesch, J., Beilecke, T., Aruffo, C.M., Weber, B., Lippmann, A., Görke, U.J., Bilke, L., 2015. Seismic and sub-seismic deformation prediction in the context of geological carbon trapping and storage, pp. 97–113. Geological Storage of CO2–Long Term Security Aspects: GEOTECHNOLOGIEN Science Report No. 22. Springer.
Krawczyk, C.M., Stiller, M., Bauer, K., Norden, B., Henninges, J., Ivanova, A., Huenges, E., 2019. 3-D seismic exploration across the deep geothermal research platform Groß Schönebeck north of Berlin/Germany. Geothermal Energy 7 (15), 1–18. https://doi.org/10.1186/s40517-019-0131-x.
LaPointe, P.R., Hermanson, J., Parney, R., Eiben, T., Dunleavy, M., Steele, K., Whitney, J., Eubanks, D., Straub, R., 2002. 3-D reservoir and stochastic fracture network modeling for enhanced oil recovery, circle ridge phosphoria/tensleep reservoir, wind river reservation, arapaho and shoshone tribes. Wyoming, tulsa, Oklahoma. US Department of Energy Technical Report, 221 DE-FG-00BC15190. https://doi.org/10.2172/815454.
Legarth, B., Huenges, E., Zimmermann, G., 2005. Hydraulic fracturing in a sedimentary geothermal reservoir: results and implications. Int. J. Rock Mech. Min. Sci. 42 (7–8), 1028–1041. https://doi.org/10.1016/j.ijrmms.2005.05.014.
Lepillier, B., Daniilidis, A., Gholizadeh, N.D., Bruna, P.O., Kummerow, J., Bruhn, D., 2019. A fracture flow permeability and stress dependency simulation applied to multi-reservoirs, multi-production scenarios analysis. Geothermal Energy 7 (24), 1–16. https://doi.org/10.1186/s40517-019-0141-8.
Li, X., 2008. An introduction to common offset vector trace gathering. CSEG Recorder 33 (9), 28–34.
Li, X.Y., 1999. Fracture detection using azimuthal variation of P-wave moveout from orthogonal seismic survey lines. Geophysics 64 (4), 1193–1201. https://doi.org/10.1190/1.1444626.
Liu, E., Martinez, A., 2012. Seismic Fracture Characterization – Concepts and Practical Applications, Education Tour Series. EAGE Publications, The Netherlands, pp. 17–18. bv. PO Box 59 3990 DB HOUTEN.
Liu, Y., 2014. AVAz and VVAZ practical analysis for estimating HTI anisotropic properties. In: Beijing 2014 International Geophysical Conference & Exposition. Society of Exploration Geophysicists and Chinese Petroleum Society, Beijing, China, pp. 1132–1135, 21-24 April 2014. https://doi.org/10.1190/IGCBeijing2014-287
Lüschen, E., Wolfgramm, M., Fritzer, T., Dussel, M., Thomas, R., Schulz, R., 2014. 3D seismic survey explores geothermal targets for reservoir characterization at Unterhaching, Munich, Germany. Geothermics 50, 167–179. https://doi.org/10.1016/j.geothermics.2013.09.007.
Lüschen, E., Görne, S., von Hartmann, H., Thomas, R., Schulz, R., 2015. 3D seismic survey for geothermal exploration in crystalline rocks in saxony, Germany. Geophys. Prospect. 63, 975–989. https://doi.org/10.1111/1365-2478.12249.
Lynn, H.B., Beckham, W.E., Simon, K.M., Bates, C.R., Layman, M., Jones, M., 1999. P-wave and S-wave azimuthal anisotropy at a naturally fractured gas reservoir, Bluebell-Altamont Field. Utah. Geophysics 64 (4), 1312–1328. https://doi.org/10.1190/1.1444636.
Marfurt, K.J., 2018. Seismic attributes as the framework for data integration throughout the oilfield life cycle. SEG Distinguished Instructor Ser. 21, 508.
Marotta, A.M., Bayer, U., Scheck, M., Thybo, H., 2001. The stress field below the NE German Basin: effects induced by the Alpine collision. Geophys. J. Int. 144 (2), F8–F12. https://doi.org/10.1046/j.1365-246x.2001.00373.x.
Marotta, A.M., Bayer, U., Thybo, H., Scheck, M., 2002. Origin of the regional stress in the North German basin: results from numerical modeling. Tectonophysics 360, 245–264. https://doi.org/10.1016/S0040-1951(02)00358-X.
McCann, T., 1998. Sandstone composition and provenance of the Rotliegend of the NE German Basin. Sediment. Geol. 116, 177–198. https://doi.org/10.1016/S0037-0738(97)00106-1.
Minsley, B.J., Burns, D.R., Willis, M.E., 2003. Fractured reservoir characterization using azimuthal AVO. Massachusetts Institute of Technology. Earth Resour. Lab. 1–20. http://hdl.handle.net/1721.1/67865.
Moeck, I., Kwiatek, G., Zimmermann, G., 2009a. Slip tendency analysis, fault reactivation potential and induced seismicity in a deep geothermal reservoir. J. Struct. Geol. 31 (10), 1174–1182. https://doi.org/10.1016/j.jsg.2009.06.012.
Moeck, I., Schandelmeier, H., Holl, H.G., 2009b. The stress regime in a Rotliegend reservoir of the Northeast German Basin. Int. J. Earth Sci. 98 (7), 1643–1654. https://doi.org/10.1007/s00531-008-0316-1.
Nadoll, P., Sośnicka, M., Kraemer, D., Duschl, F., 2019. Post-Variscan structurally-controlled hydrothermal Zn-Fe-Pb sulfide and F-Ba mineralization in deep-seated Paleozoic units of the North German Basin: a review. Ore Geol. Rev. 106, 273–299. https://doi.org/10.1016/j.tecto.2004.10.009.
Norden, B., Bauer, K., Krawczyk, C.M., 2023. From pilot site knowledge via integrated reservoir characterization to utilization perspectives of a deep geothermal reservoir: the 3D model of Groß Schönebeck (North German Basin). Geothermal Energy 11 (1), 1–44. https://doi.org/10.1186/s40517-022-00242-2.
Pussak, M., Bauer, K., Stiller, M., Bujakowski, W., 2014. Improved 3D seismic attribute mapping by CRS stacking instead of NMO stacking: application to a geothermal reservoir in the Polish Basin. J. Appl. Geophy. 103, 186–198. https://doi.org/10.1016/j.jappgeo.2014.01.020.
Reinhardt, H.G., 1993. Structure of Northeast Germany: regional depth and thickness maps of Permian to Tertiary intervals compiled from seismic reflection data. Generation, Accumulation and Production of. Europe's Hydrocarbons III. Springer, Berlin, Heidelberg, pp. 155–165. https://doi.org/10.1007/978-3-642-77859-9_13.
Roth, F., Sperner, B., Jarosinski, M., Krupsky, Y., Weigold, G., Bäbler, H., Müller, B., 1997. Orientation of tectonic stress from boreholes in NE Germany. Poland and the Western Ukraine. Terra Nostra 11 (1), 18–120.
Röckel, T., Lempp, C., 2003. Der spannungszustand im norddeutschen becken. Erdöl Erdgas Kohle 119 (2), 73–80.
Rüger, A., 1997. P-wave reflection coefficients for transversely isotropic models with vertical and horizontal axis of symmetry. Geophysics 62 (3), 713–722. https://doi.org/10.1190/1.1444181.
Rüger, A., 1998. Variation of P-wave reflectivity with offset and azimuth in anisotropic media. Geophysics 63 (3), 935–947. https://doi.org/10.1190/1.1444405.
Scheck, M., Bayer, U., Lewerenz, B., 2003. Salt redistribution during extension and inversion inferred from 3D backstripping. Tectonophysics 373 (1–4), 55–73. https://doi.org/10.1016/S0040-1951(03)00283-X.
Schmelzbach, C., Greenhalgh, S., Reiser, F., Girard, J.-F., Bretaudeau, F., Capar, L., Bitri, A., 2016. Advanced seismic processing/imaging techniques and their potential for geothermal exploration. Interpretation 4 (4), SR1–SR18. https://doi.org/10.1190/INT-2016-0017.1.
Shapiro, S.A., Kaselow, A., 2005. Porosity and elastic anisotropy of rocks under tectonic stress and pore-pressure changes. Geophysics 70, 27–38. https://doi.org/10.1190/1.2073884.
Shen, F., Zhu, X., Toksöz, M.N., 2002. Effects of fractures on NMO velocities and P-wave azimuthal AVO response. Geophysics 67 (3), 711–726. https://doi.org/10.1190/1.1484514.
Shouli, Q., Yuxin, J., Xin, W., Xiuling, W., Xinrong, C., Guoqiang, S., 2007. Fracture detection by using full azimuth P wave attributes. Appl. Geophys. 4 (3), 238–243. https://doi.org/10.1007/s11770-007-0032-9.
Stiller, M., Bauer, K., Henninges, J., Norden, B., Krawczyk, C., Huenges, E., 2018. 3D seismic survey at the geothermal research platform Groß Schönebeck /Germany. EAGE Conference, p. 5.https://doi.org/10.3997/2214-4609.201801627.
Stober, I., Bucher, K., 2014. Hydraulic and hydrochemical properties of deep sedimentary aquifers of the Upper Rhine Graben, Europe. Geofluids 15 (3), 464–482. https://doi.org/10.1111/gfl.12122.
Stober, I., Bucher, K., 2015. Hydraulic conductivity of fractured upper crust: insights from hydraulic tests in boreholes and fluid-rock interaction in crystalline basement rocks. Geofluids 16, 161–178. https://doi.org/10.1002/9781119166573.ch15.
Suo, C., Peng, S., Chang, S., Duan, R., Wang, G., 2012. A new calculating method of the curvature to predicting the reservoir fractures. Procedia Environ. Sci. 12, 576–582. https://doi.org/10.1016/j.proenv.2012.01.320.
Thomsen, L., 1986. Weak elastic anisotropy. Geophysics 51, 1954–1966. https://doi.org/10.1190/1.1442051.
Treadgold, G., Sicking, C., Sublette, V., Hoover, G., 2008. Azimuthal processing for fracture prediction and image improvement. SEG Technical Program Expanded Abstracts 2008 Society of Exploration Geophysicists, pp. 988–992.https://doi.org/10.1190/1.3063803.
Tsvankin, I., 1997. Reflection moveout and parameter estimation for horizontal transverse isotropy. Geophysics 62 (2), 614–629. https://doi.org/10.1190/1.1444170.
Tsvankin, I., Grechka, V., 2011. Seismology of azimuthally anisotropic media and seismic fracture characterization. Soci. Explorat. Geophys, p. 1–122. https://doi.org/10.1190/1.9781560802839.refs.
Tsvankin, I., 2012. Seismic signatures and analysis of reflection data in anisotropic media. Soc. Explorat. Geophys, p. 7–161. https://doi.org/10.1190/1.9781560803003.refs.
Upadhyay, S.K., 2013. Seismic Reflection Processing: with Special Reference to Anisotropy. Springer Science & Business Media. Springer-Verlag, Berlin Heidelberg, pp. 77–130. https://doi.org/10.1007/978-3-662-09843-1.
Vannucci, P., 2018. General anisotropic elasticity. Anisotropic Elasticity. Springer, Singapore, pp. 19–73. https://doi.org/10.1007/978-981-10-5439-6_2.
von Hartmann, H.von, Beilecke, T., Buness, H., Musmann, P., Schulz, R., 2015. Seismische exploration für tiefe Geothermie. Geol. Jb. B 104 27, 171 figures7 tables; Hannover.
Wadas, S.H., von Hartmann, H., 2022. Porosity estimation of a geothermal carbonate reservoir in the German Molasse Basin base on seismic amplitude inversion. Geotherm. Energy 10 (1), 13. https://doi.org/10.1186/s40517-022-00223-5.
Wadas, S.H., Krumbholz, J.F., Shipilin, V., Krumbholz, M., Tanner, D.C., Buness, H., 2023. Advanced seismic characterization of a geothermal carbonate reservoir – insight into the structure and diagenesis of a reservoir in the German Molasse Basin. Solid Earth 14 (8), 871–908. https://doi.org/10.5194/se-14-871-2023.
Wang, N., Mantagner, J.-P., Fichtner, A., Capdeville, Y., 2013. Intrinsic versus extrinsic seismic anisotropy: the radial anisotropy in reference Earth models. Geophys. Res. Lett. 40, 1–5. https://doi.org/10.1002/grl.50873.
Wang, J., Zheng, Y., Perz, M., 2007. VVAZ vs. AVAZ: practical implementation and comparison of two fracture-detection methods. SEG Technical Program Expanded Abstracts 2007. Society of Exploration Geophysicists, pp. 189–193.
Wawerzinek, B., Buness, H., von Hartmann, H., Tanner, D.C., 2021. S-wave experiments for the exploration of a deep geothermal carbonate reservoir in the German Molasse

Basin. Geotherm. Energy 9 (1), 1–21. https://doi.org/10.1186/s40517-021-00189-w.
Wenke, A., Kreuter, H., Gall, W., Gutekunst, S., Rohrer, L., Zühlke, R., 2010. First steps in the development of a new geothermal field in the Northern part of the Upper Rhine Graben, Germany. In: Proceedings Word Geothermal Congress: Bali, Indonesia, pp. 25–29.
World Stress Map, 2000. http://www-wsm.physik.uni-karlsruhe.de. 6th December 2022.
Yilmaz, Ö., 2001. Seismic Data Analysis: Processing, Inversion, and Interpretation of Seismic Data. Society of Exploration Geophysicists, pp. 271–324.
Zhang, J., Qi, J., Zeng, Y., Marfurt, K., Slatt, R., 2020. Azimuthal anisotropy analysis applied to naturally fractured unconventional reservoirs: a Barnett Shale example. Interpretation 8 (4), SP13–SP29. https://doi.org/10.1190/INT-2019-0206.1.
Ziesch, J., Tanner, D.C., Krawczyk, C.M., 2019. Sub-seismic pathway prediction by three-dimensional structural restoration and strain analysis based on seismic interpretation. Am. Assoc. Pet. Geol. Bull. 103 (10), 2317–2342. https://doi.org/10.1306/0130191516517255.
Zimmermann, G., Blöcher, G., Reinicke, A., Brandt, W., 2011. Rock specific hydraulic fracturing and matrix acidizing to enhance a geothermal system—concepts and field results. Tectonophysics 503 (1–2), 146–154. https://doi.org/10.1016/j.tecto.2010.09.026.